Characterization of *In Situ* Prepared Nano-Hydroxyapatite/ Polyacrylic Acid (HAp/PAAc) Biocomposites

G. S. El-Bahy,[1] E. M. Abdelrazek,[2] M. A. Allam,[1] A. M. Hezma[1]

[1]*Spectroscopy Department, Physics Division, National Research Centre, Dokki, Giza, Egypt*
[2]*Physics Department, Faculty of Science, Mansoura University, Mansoura 35516, Egypt*

Received 6 June 2010; accepted 20 February 2011
DOI 10.1002/app.34413
Published online 12 July 2011 in Wiley Online Library (wileyonlinelibrary.com).

ABSTRACT: Nanoparticles hydroxyapatite (HAp) was prepared via an *in situ* biomimetic process with polyacrylic acid (PAAc) as a host polymeric material. Fourier transform infrared spectroscopy, transmission electron microscopy, scanning electron microscopy, X-ray diffraction, thermogravimetric analysis, and differential scanning calorimetry were used to test the physical and chemical characteristics of biocomposites. The formation of HAp is confirmed by energy dispersion X-ray analysis. Chemical binding between inorganic HAp and PAAc was investigated and discussed. HAp formation was initiated through the interaction of Ca^{2+} ions with the negative side groups of the polymer surface. The results showed that the biocomposites were formed with good homogeneity and thermal stability. Nanoparticles of HAp were uniformly distributed in the polymeric matrices. The resulting new materials are hoped to be applicable in the biomedical fields. © 2011 Wiley Periodicals, Inc. J Appl Polym Sci 122: 3270–3276, 2011

Key words: nanoparticles; hydroxyapatite; biocomposites; FTIR; X-ray; TEM

INTRODUCTION

Since the discovery of the bone tissue of mammal's hydroxyapatite (HAp), great efforts have been made to develop phosphate ceramics as a potential implant material.[1,2] Artificially synthesized HAp and/or nano-HAp proved to be a successful substitute for natural HAp. Besides being biocompatible and nontoxic, this material exhibits unique osteoinductive properties.[3] Up to now, the HAps did not have thermal properties necessary for this type of application. Low toughness of HAp limited application of this material as implants.[4–6] One of the solutions of the problem is the development of ceramic/metal and ceramic/polymer biocomposites[7–10] widely used in medicine and stomatology for repair of bone tissue. Polymer phase can have the same chemical composition as the polymer in bone tissue (collagen) but could be synthesized as well.[11–15] Special attention has been focused on biodegradable polymers that have been successfully applied so far in medicine.[12,13,16]

Also, bioactive biomaterials such as HAp have been known to form a bioactive bone layer spontaneously on their surfaces and bond to bone through the apatite layer.[14] Therefore, it is generally accepted that an essential prerequisite for an artificial bone biomaterial to directly bond to living bone tissue is the formation of a bone-like apatite layer on its surface when implanted.[15–17]

Current research efforts have thus focused on biocomposites of synthetic polymers and HAp formed using *in situ* mineralization techniques. A few polymeric additives such as PAAc have been investigated as suitable organic additives.[18] PAAc has been found to accelerate the nucleation of HAp from calcium and phosphate solutions. The ionizable carboxylate functionalities of PAAc provide high affinity to calcium ions from HAp.[19,20] The presence of PAAc in biomimetic HAp significantly alters its surface properties.

In this study, biocomposite films of HAp and polyacrylic acid (PAAc) were synthesized *in situ* with different concentrations of nanoparticles HAp. Nano-HAp was also synthesized in absence of polymer. The interfacial interaction between HAp and PAAc has been investigated using FTIR and X-ray spectroscopic techniques, SEM and TEM micrscopy. Also, thermal properties were investigated by TGA and DSC analysis.

EXPERIMENTAL

Materials

The chemicals used were polyacrylic acid (PAAc), $w_x = 35\%$ solution in water with $M_w = 100{,}000$ from Aldrich (Lot No. 523925), calcium nitrate A. R

Correspondence to: A. M. Hezma (ahezma@yahoo.com).

($Ca(NO_3)_2{\cdot}4H_2O$) from WINLAB, UK (Lot No. 121065), and diammonium hydrogen phosphate $(NH_4)_2.HPO_4$ from SISCO Research Laboratories, India (Lot No. 0149174). All chemicals were used as received.

Preparation of nano-HAp in PAAc

Casting method used for preparation of biocomposite films consists of PAAc filled by nanoparticles of hydroxyapatite *in situ*. Certain amount of PAAc was dissolved in double-distilled water to obtain solution of PAAc, and $Ca(NO_3)_2$ was dissolved also in distilled water to remove all protons from the carboxylic group obtaining carboxylate groups and then dropped to PAAc solution, the pH was adjusted between 10 and 12 by adding drop by drop NH_4OH constant stirring at room temperature for 4 h to ensure completely formation of $Ca^{2+}{\cdot}(NH_4)_2{\cdot}HPO_4$ solution was added drop by drop at the same pH at room temperature stirred for 7 h until turbidity appears in the solution due to the formation of amorphous calcium phosphate. The prepared samples dried at room temperature and films of thickness ranging from 1 to 2 mm were obtained.

The formation of hydroxyapatite nanoparticles was assumed to follow the equation:

$$10Ca(NO_3)_2 \cdot 4H_2O + 6(NH_4)_2 \cdot HPO_4 + 8NH_4OH \rightarrow Ca_{10}(PO_4)_6 \cdot (OH)_2 + 20NH_4NO_3 + 46H_2O \quad (1)$$

HAp nanoparticles were prepared without PAAc as mentioned before to obtain optimum biocomposites films from the nanoparticles of HAp with PAAc ratio was maintained at different concentrations (S_0, S_2, S_3, S_4, S_5, S_6, S_7, and S_{10}) as maintained in Table I.

Experimental analysis

Fourier Transform Infrared Spectrophotometer (FTIR) measurements were carried out using the single beam (FTIR-400, JASCO, Japan) in the spectral range of 4000–400 cm^{-1} at room temperature with scanning speed of 2 mm s^{-1} and 2 cm^{-1} resolution, respectively. Forty scan per spectrum were done on a thin film of samples dried at about 40°C. FTIR measurements were used to determine the bonding between the HAp phase and PAAc phases.

TABLE I
The Particle Size of HAp in the Nanosize

	Sample HAp/PAAc	$2\theta = 25.9$	$2\theta = 32.94$
		β (nm)	β (nm)
S_2	20/80	–	53.15
S_3	30/70	–	53.39
S_4	40/60	–	53.1
S_5	50/50	41.50	53.21
S_6	60/40	41.47	52.63
S_7	70/30	41.39	53.19
S_{10}	100/0	41.38	53.21

X-ray diffraction analysis were studied by using DIANO corp.-USA equipped with Cu Kα radiation at $\lambda = 1.5406$ Å, the Bragg angle (2θ) in the range of 4–70°, step size = 0.02, and step time 0.4s at room temperature.

The size of the crystallites responsible for the Bragg reflection of the (002) and (300) planes were determined using Scherrer equation:

$$d = \frac{K\lambda}{\beta \cos\theta} \quad (2)$$

where d is the crystalline diameter in nm, β is the peak width at half-maximum peak height in radians, λ is the X-ray wavelength, typically 1.54 Å, and θ is the Bragg angle.[21]

The morphology of the films was characterized by scanning electron microscopy using (JEOL 5300, Tokyo, Japan), operating at 30 kV accelerating voltage. Surface of the samples were coated with a thin layer of gold (3.5 nm) by the vacuum evaporation technique to minimize sample charging effects due to the electron beam. The Ca/P ratio was determined by EDX analysis from SEM.

The DSC of the prepared films was conducted using an instrument type (SDT Q600 V20.5 Build 15) from room temperature to 400°C with a heating rate of 10°C/min in an aluminum ban.

A Shimadzu TGA-50H was used for the thermogravimetric analysis of the samples. A small amount (4–10 mg) of the sample was taken for the analysis and the samples heated from room temperature to 400°C at a rate of 10°C/min in nitrogen atmosphere in platinum cell.

Transmission electron microscopy (TEM) was used to detect the morphology of the HAp nanoparticles and that in composite particles. TEM observation and the corresponding selected area electron diffraction were performed on a JEOL JEM-1230 electron microscope at accelerating voltage of 150 kV. TEM samples were deposited on thin amorphous carbon films supported on copper grids from ultrasonically processed ethanol solution of the products and used to observe the morphology of the nanoparticles and the nanobiocomposites. A drop of the solution was placed on a copper grid that was left to dry before transferring into the TEM sample chamber.

RESULTS AND DISCUSSION

Fourier transform infrared analysis

Figure 1(a,b) shows FTIR absorption spectra of the prepared HAp and HAp/PAAc biocomposite films

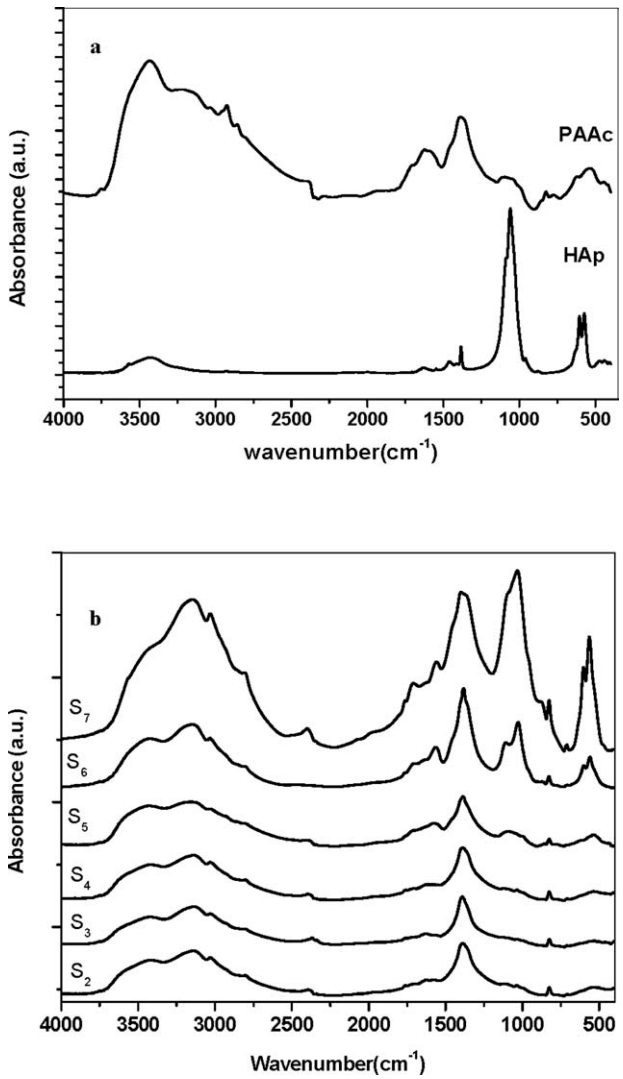

Figure 1 FTIR of (a) prepared HAp and PAAc, (b) HAp/PAAc biocomposite films *in situ* with different concentrations of nano-Hap.

in situ with different concentrations of HAp, respectively, recorded at the room temperature in the spectral region 4000–400 cm^{-1}.

For pure nano-HAp [Fig. 1(a)], it is clear that the broad absorption band between 2800 and 3700 cm^{-1} is attributed to the OH stretch of $Ca(OH)_2$, HAp and NH stretch of NH_4^+ from $(NH_4)_2 \cdot HPO_4$.[22,23] This broad band indicates the complete loss of water dehydration of $Ca(OH)_2$.[22–24]

The bending mode of H_2O is observed at 1637 cm^{-1}, the sharp band at 1384 cm^{-1} is assigned to *N*—O stretch of NO_3^-. The PO_4^{3-} stretching mode is positioned at 1031cm^{-1} as a main sharp band. There are other bending modes of PO_4^{3-} at 602 and 563 cm^{-1}, respectively. The small band at 874 cm^{-1} is also assigned to NO_3^- bending mode.[21–25]

For the spectra of pure PAAc [Fig. 1(b)], the observation of the characteristic stretching band of carboxylic group C=O at 1703 cm^{-1}. The band at 1387 cm^{-1} is assigned to CH_3 bending mode with scissoring and bending vibration of (—CH_2—) and (—CH—CO—) groups. The bands at 1096 and 825 cm^{-1} due to out of plane C—H bonds. The band at 725 cm^{-1} is attributed to (—C—CH_2—) rocking mode.[25,26,27]

For the biocomposites films [Fig. 1(c)] showed that the dissociated carboxylate groups, also show a band at around 1387 cm^{-1}, which has been assigned to symmetric stretching of carboxylate group.[25] This suggested that the carboxylate groups dissociate and chelate with Ca atoms present on surface of HAp nanoparticles *in situ*.[25]

It is clear that the bands 1031, 602, 563, and 1387 increased with increasing HAp concentration this is due to the fact that the carboxylate groups of PAAc chelates with Ca^{2+} present on surface of *in situ* HAp and also, the carboxylate groups present on surface of *in situ* HAp could also make hydrogen bond with carboxylate groups of nano-HAp/PAAc biocomposites.[25]

A new band at about 1575cm^{-1} is assigned to the formation of chelation complex from carboxylic group of PAAc and Ca ion from HAp[25] which increased with adding HAp. The presence of phosphate, carbonate, and chelation complex on all biocomposites is apparent also. Scheme 1 suggested the bond between Ca^{2+} in HAp/PAAc biocomposites.

X-ray diffraction analysis

Figure 2 shows XRD for pure HAp. All peaks are indexed to hexagonal lattice of $Ca_5(PO_4)_3(OH)$ crystal. The wide and high peaks reveal that the pure HAp has a very small size (nanoparticles).[25,28]

The d spacing, intensities, and lattice parameters for the hexagonal HAp are compared with JCPDS Card (data file No. 9-432 and 73-294) standard for HAp in Table II.

The presence of diffraction peaks on the spectrum at 2θ = 25.95, 30.22, 31.51, 32.94, 34.09, 39.70, 46.78,

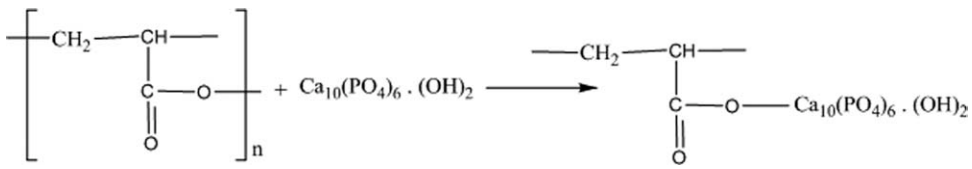

Scheme 1 The suggested chemical interaction bond between nano-HAp and PAAc.

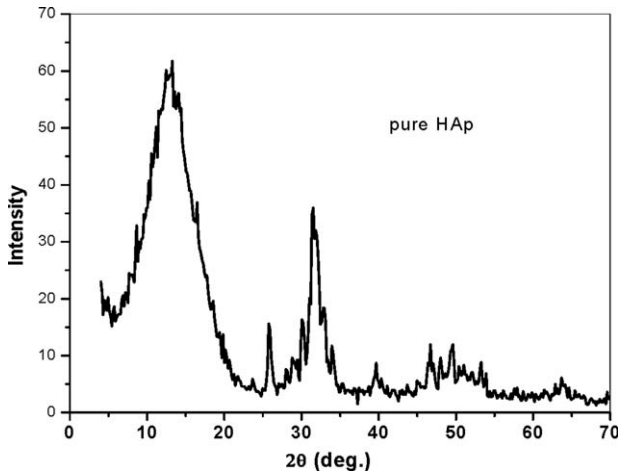

Figure 2 XRD of nano-Hap.

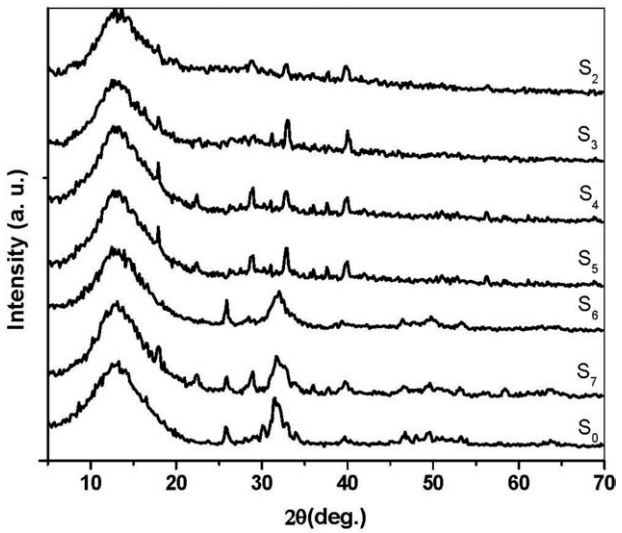

Figure 3 XRD patterns of HAp/PAAc biocomposites at different ratios.

48.00, and 49.62 for the planes, (002), (210), (211), (300), (202), (212), (222), (312), and (213), respectively, may be indicate that the basic apatite phase is decomposed into different crystalline phases, these phases may be classified to α-$Ca_3(PO_4)_2$, β-$Ca_3(PO_4)_2$, $Ca_4P_2O_4$, and $Ca_4P_2O_3$ which were identified among the original apatite. These calcium phosphate phases are well known as bioactive and biocompatible materials.[29]

From the XRD patterns for pure PAAc and biocomposites (Fig. 3) after adding nanoparticles of HAp to the polymer, some changes in the main structure of these biocomposites are found.[25,30] However, some peaks have slightly broadened, indicating that the crystallinity of the apatite layer formation on the surface of the biocomposites was lower than that of pure HAp specially the two peaks at $2\theta = 25.90$ and $2\theta = 32.94$ which decreased and may be disappeared with decreasing HAp, which might indicate that PAAc in the biocomposite films was covered by the deposited apatite layer on the surface of biocomposite.

On the other hand, the intensity of some peaks for the polymer was decreased which may be due to the interaction between Ca^{2+} and PO_4^{3-} with the polymeric matrix, resulting the formation of the apatite layers and/or HAp crystals on the surface of these composites. Table II shows the particle size calculated by the eq. (2).

TABLE II
***d* Spacing, Intensities, and Lattice Parameters of HAp Nanopowder**

2θ (deg.)	*d* (Å)	Intensity (%)	hkl
25.90	3.44	42.4	002
30.22	2.94	42.4	210
31.51	2.83	100	211
32.94	2.71	49	300
34.09	2.62	27	202
39.76	2.26	21.7	212
46.78	1.94	28.6	222
48.00	1.89	22.6	312
49.62	1.83	28.6	213

Differential scanning colorimetry

Figure 4 shows the DSC curves for the prepared films. As it can be seen from these curves and for pure PAAc, there are two exothermic peaks at 50°C and 128°C, in addition the curves shows exothermic peak at 229.18°C.

It is clear that, after adding HAp up to S_4 sample the same trend for these samples with increasing of the melting point of the films with increasing of the degree of crystallinity (area under the peak) with nearly disappearance of all peaks $\geq S_6$ samples this due the nature of HAp as shown in Table III.

In the DSC curves and the table of these samples ($\leq S_6$ samples), the first endothermic peak at 50°C can be attributed to the small amount of water that is always present in the HAp/PAAc biocomposite unless it is carefully vacuum dried. The second endothermic peak at 128°C can be attributed to formation of PAAc anhydride. The third exothermic peak at 229.18°C can be ascribed to the degradation of corresponding PAAc anhydride. These results are in good agreement with the data reported in the literature[30,31] especially those for the low molecular weight of PAAc which equal to 100,000 as reported by Cardenas et al.[30] However, the slight shift in the peak positions in the DSC curve (form S_2 to S_4) may be attributed to increase HAp ratio. This indicates that the addition of HAp increases the thermal stability.

Thermogravimetric analysis

Figure 5 shows the thermogravimetric analysis (TGA) curves of the pristine HAp, PAAc, and

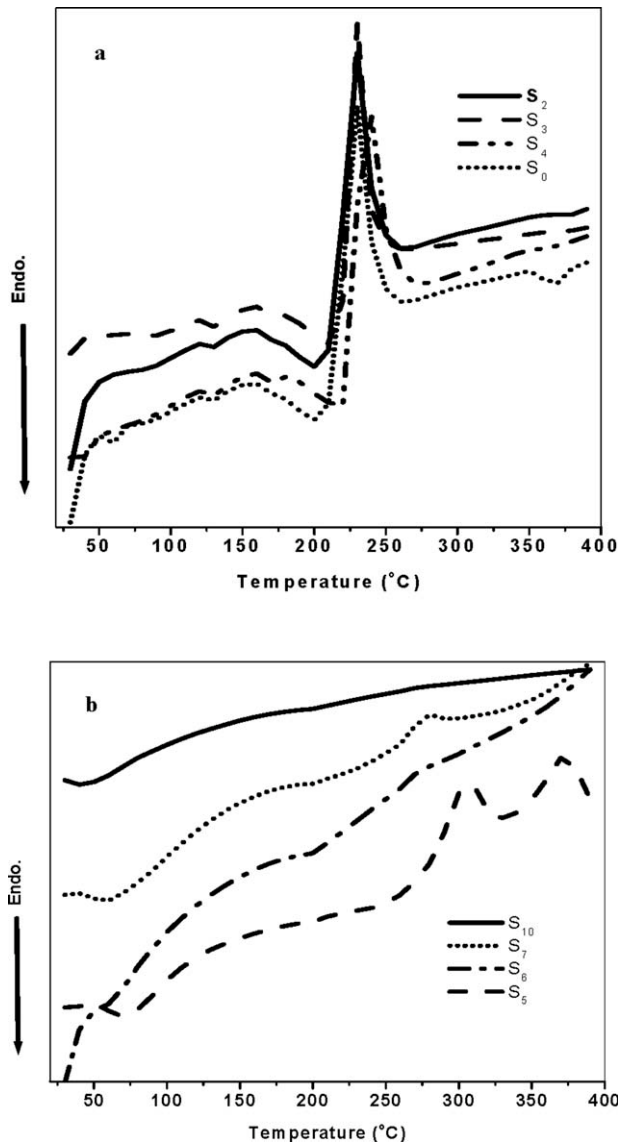

Figure 4 DSC curves of prepared HAp, PAAc, and HAp/PAAc biocomposite films with different concentrations of nano-HAp (a,b).

composite films with different concentrations of HAp. For comparison, TGA curves of pure HAp and pure PAAc are also shown in Figure 5.

TGA curves for the samples $\leq S_7$ samples reveal three main weight loss regions. The first region at a temperature of 80–200°C is due to the evaporation of physical weakly and chemically strongly bound

TABLE III
T_W, T_g, T_m, and T_d for Pure PAAc and Its Biocomposites with HAp

		T_W	T_g	T_m	T_d
S_0	0/100	50	128	229	164
S_2	20/80	40	128	227	167
S_3	30/70	55	127	238	166
S_4	40/60	48	–	305	373

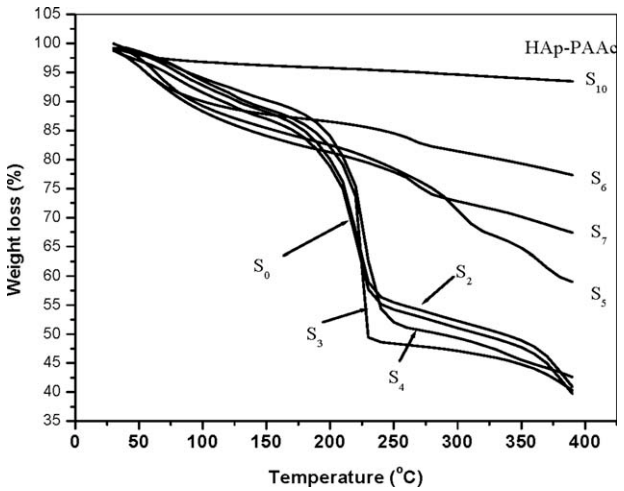

Figure 5 TGA curves of nano-HAp, PAAc, and HAp/PAAc biocomposites.

H_2O, the weight loss of the membrane is about 5%. The second transition region around 200–250°C is due to the degradation of PAAc polymer, the total weight loss corresponds to this stage about 25–47%. The transition peak of third stage after 300°C is due to the cleavage backbone of polymer.

Overall, the degradation peaks of the crosslinked films are less intense and shifted to higher temperatures in the temperature range of 200–300°C (pure polymer film shows larger weight loss in this temperature range).[31] It can be seen that the improved thermal stability is probably due to the additive effect of HAp filler and the chemical crosslink reaction between the polymer and HAp. Table IV shows the results of weight loss (%) of the HAp/PAAc biocomposite at various temperatures.

Transmission electron microscope

Figure 6(a–c) shows the transmission electron microscope (TEM) micrographs of pure HAp (image a), S_7 sample (image b), and S_6 sample (image c). Figure 6(a) indicates that the nanoparticles of HAp are in the nanometer grad (15 ± 5 nm). These results are

TABLE IV
The Weight Loss (%) of the HAp/PAAc Biocomposite at Different Temperatures

	Sample Hap/PAAc	Temperature (°C)				
		150	200	250	300	390
S_0	0/100	11.5	21	45	48	59
S_2	20/80	11.5	21	45	48	59
S_3	30/70	11.3	18.5	51.5	53	60
S_4	40/60	9.2	16	48	51	47.5
S_5	50/50	14.5	17.5	21.5	29	41
S_6	60/40	13	13.5	15.5	19	23
S_7	70/30	16	19	22	27	32.5
S_{10}	100/0	4	4.4	4.5	5.5	6.5

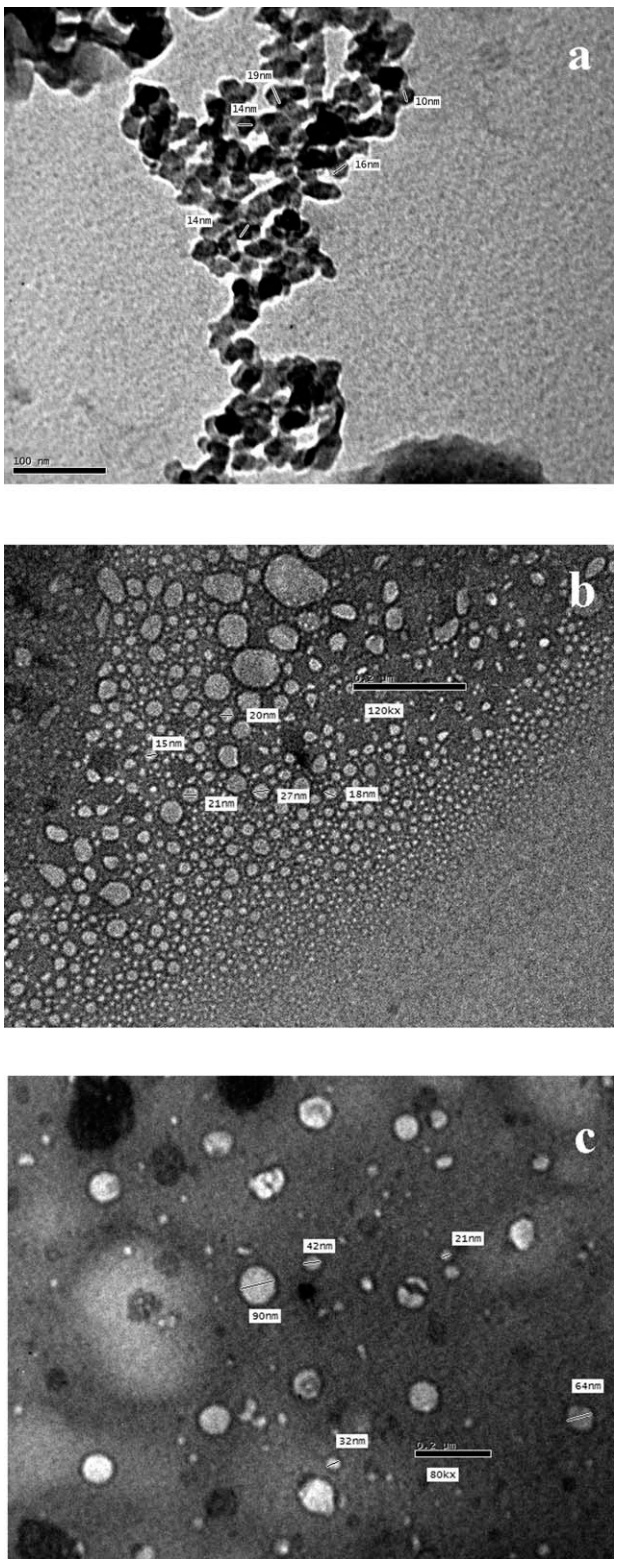

Figure 6 TEM micrographs for (a) prepared HAp, (b) 70 HAp/30 PAAc, (c) 60 HAp/40 PAAc.

in good agreement with the micrograph observation in literature.[32,33]

All the biocomposites samples showed nanosized morphology with an increase in the particle size from (18 ± 2 nm) to (49 ± 10 nm) for S_7 sample and S_6 sample respectively, with good modify and improve dispersion of HAp in the polymer which similar in chemical and structure with homogenous distribution in polymer matrix.

Scanning electron microscope

Morphological results from scanning electron microscope (SEM) investigation of S_7 and S_6 samples are shown in Figure 7(a,b). The morphology of these microcrystals reveal pores of approximately 5 μm size and seem to be connected to form continues network separated by region of the polymer. These pores may be an advantage for circulation of physiological fluid when it is used as bioactive material.[34]

EDX data [Fig. 8(a)] for S_7 sample and [Fig. 8(b)] for S_6 sample showed that the Ca/P ratio is approximately 1.63 and 1.66 for S_7 and S_6 samples, respectively. It is known that Ca/P ratio in human bone is 1.67.[35]

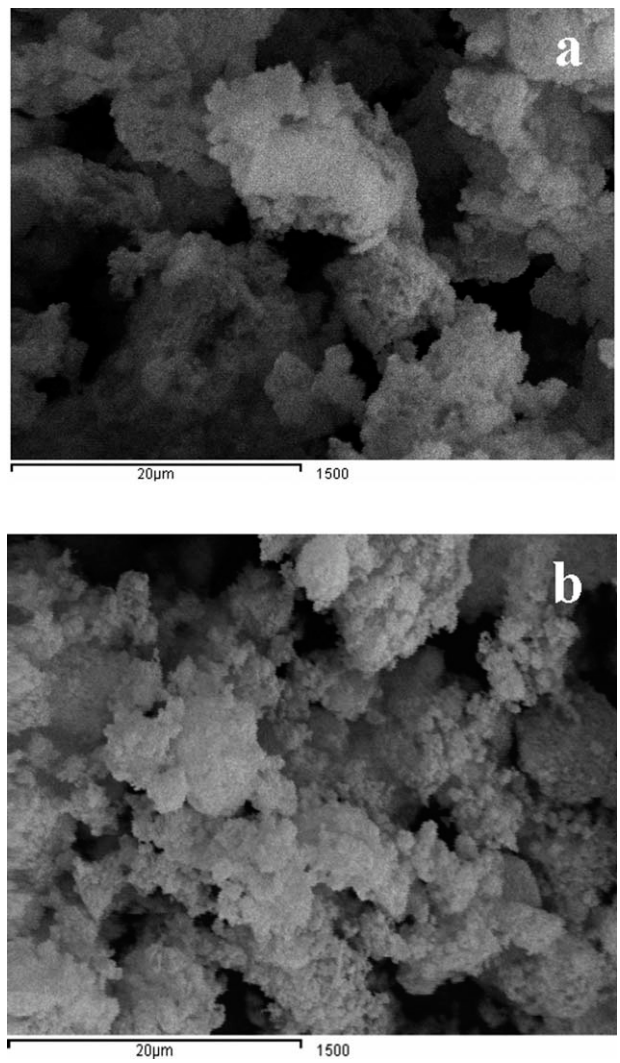

Figure 7 SEM micrographs for (a) 70 HAp/30PAAc, (b) 60HAp/40PAAc.

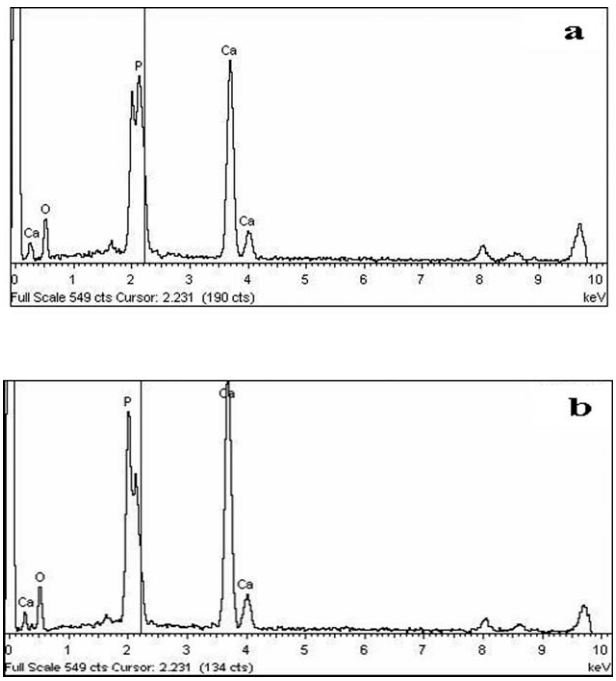

Figure 8 EDX data for (a) 70HAp/30PAAc, (b) 60 HAp/40 PAAc.

CONCLUSIONS

Nanoparticles hydroxyapatite (HAp/PAAc) composites were prepared via an *in situ* biomimetic process and formation of hydroxyapatite is confirmed by energy dispersion X-ray (EDX) analysis. Chemical binding between inorganic HAp and PAAc was initiated through the interaction of Ca^{2+} ions with the negative side groups of the polymer surface and formed composite were formed with good homogeneity and thermal stability. Nanoparticles of HAp were uniformly distributed in the polymeric matrices. The resulting new materials may be applicable in the biomedical fields.

References

1. Katz, J. L.; Harper, R. A. Encyclopedia of Materials Science and Engineering; Oxford, 1986; p 475.
2. Hienderauer, G. G.; McGee, T. D.; Kudej, R. K.; Ceramic Bull 1991, 70, 1010.
3. Zambonin, G.; Grano, M. Biomaterials 1995, 16, 397.
4. Lu, L.; Mikos, A. MRS Bull 1996, 21, 28.
5. Ruys, A. J.; Wei, M.; Sorrell, C. C.; Dickson, M. R.; Brandwood, A.; Milthorpe, B. K. Biomaterials 1995, 16, 409.
6. Kane, R. J.; Converse, G. L.; Roeder, R. K. J Mech Behav Biomed 2008, 1, 261.
7. Li, J.; Fartash, B.; Hermanson, L. Biomaterials 1995, 16, 417.
8. Labella, R.; Braden, M.; Deb, S. Biomaterials 1994, 15, 1197.
9. Hench, L. L. J Am Ceram Soc 1991, 74, 1487.
10. Liu, C.-Z. J Bionic Eng Supp 2008, 5, 1.
11. Wang, M.; Deb, S.; Tanner, K.; Bonþeld, W, Proceedings of 7th European Conference on Composite Materials, London, 1996; p 455.
12. Törmäla, P. Adv Mater 1992, 4, 589.
13. Ristich, C.; Plavsic, M.; Goosen, M.; Sajc, L.; Antonovic, D.; Bugarski, B. J Serb Chem Soc 1996, 61, 311.
14. Ripamonti, U.; Duneas, N. MRS Bull 1996, 21, 36.
15. Rodrigues, L. S.; Vallet-Regi, A. M.; San-Roman, J. J Biomed Mater Res 1996, 30, 515.
16. Converse, G. L.; Yue, W.; Roeder, R. K. Biomaterials 2007, 28, 927.
17. Roeder, R. K.; Converse, G. L.; Kane, R. J.; Yue, W. JOM 2008, 60, 38.
18. Katti, K.; Gujjula, P. Proceedings of 15th ASCE Engineering Mechanics Conference, New York, NY, 2002.
19. Bonfield, W.; Ducheyne, P.; Lemons, L. E. Ann N Y Acad Sci 1998, 523, 173.
20. Verma, D.; Katti K.; Katti, D. J Biomed Mater Res 2006, 77, 59.
21. Abdelrazek, E. M.; Damrawi, G.; Al-Shahawy, A. Physica B 2010, 405, 808.
22. Anee, T. K.; Ashok, M.; Palanichamy, M.; Kalkura, N. Mater Chem Phys 2003, 80, 725.
23. Liu, Y.; Hou, D.; Wang, G. Mater Chem Phys 2004, 86, 69.
24. Caixia Lei, C.; Liao, Y.; Feng, Z. Biomed Mater 2009, 4, 35010.
25. Katti, K. S.; Turlapati, P.; Verma, D.; Bhowmik, R.; Gujjula, P. K.; Katti, D. R. Am J Biochem Biotechnol 2006, 2, 73.
26. Ge, Y.; Zhang, S. J Nanosci Nanotechnol 2009, 9, 1287.
27. Sailaja, G. S.; Velayudhan, S.; Sunny, M. C.; Sreenivasan, K.; Varma, H. K.; Ramesh, P. J Mater Sci 2003, 38, 3653.
28. Kealley, C.; Elcombe, M.; Riessen, A. V.; Nissan, B. B. Physica B 2006, 385, 496.
29. Banerjee, A.; Bandyopadhyay, A.; Bose, S. Mater Sci Eng C 2007, 27, 729.
30. Cardenas, G.; Munoz, C.; Carbacho, H. Eur Polym Mater 2000, 36, 1091.
31. Moharram, M. A.; Allam, M. A. J Appl Polym Sci 2007, 105, 3220.
32. Fenglan, X. U.; Yubao, L. J Mater Sci 2004, 39, 5669.
33. Mollazadeh, S. J Ceram Inter 2007, 33, 1579.
34. Zhang, Y.; Yokogawa, Y.; Feng, X.; Tao, Y.; Li, Y. Ceram Inter 2010, 36, 107.
35. Cengiz, B.; Gokce, Y. Colloids Surf 2008, 322, 29.